15th International Symposium on Computer Methods in Biomechanics and Biomedical Engineering
and
3rd Conference on Imaging and Visualization
CMBBE 2018
P. R. Fernandes and J. M. Tavares (Editors)

QUASI AUTOMATED RECONSTRUCTION OF THE FEMUR FROM BI-PLANAR X-RAYS

F. Girinon[*], **L. Gajny**[*], **S. Ebrahimi**[*], **L. Dagneaux**[†], **P. Rouch**[*], **W. Skalli**[*]

[*]Arts et Metiers ParisTech, IBHGC
151 bd de l' hopital, 75013 Paris, France
Corresponding author: francois.girinon@ensam.eu

[†]Department of Orthopaedic Surgery, CHU Montpellier
191, avenue du Doyen Gaston Giraud 34295 Montpellier, France

Keywords: Biomechanics, Biomedical Imaging, Computer Methods, Femur, Bi-planar X-rays, 3D reconstruction.

Abstract: *3D reconstruction from low dose Bi-Planar X-Rays (BPXR) has become common practice in clinical routine. The aim of this study is to partially automate the process for the femur, thus decreasing reconstruction time and increasing robustness.*
As a training set 50 femurs were segmented from CT scans together with 120 BPXR reconstructions. From this data and 8 digitized landmarks, bony shapes are initialized through Gaussian Process Regression (GPR). This initial solution is retro-projected on both x-rays and automatically adjusted based on an adapted minimal path algorithm (MPA).
The proposed method has been applied to the femur and evaluated comparing 20 cadaveric CT scans (0.75 mm resolution) from which we have simultaneously generated digital radiographs and their bony surfaces. The projected Euclidean distances between femur reconstructions and the segmented CT data were on average 1.0 mm with a Root Mean Square Error (RMSE) of 0.8 mm. Femoral torsions errors were also assessed: the bias was lower than 0,1° with a 95% confidence interval of 4.8°.
Such a method drastically improves 3D reconstructions from BPXR since it allows to obtain a fast and reliable reconstruction without any further manual adjustments, essential in clinical routine.

1. INTRODUCTION

Three-dimensional reconstruction of the skeleton from bi-planar X-rays has become common practice in clinical routine. Compared to standard imaging techniques such as Computed Tomography (CT-scan), these low dose images modalities are faster and enable to obtain the 3D surface of the bones in standing position. Femur reconstructed from bi-planar X-rays is one of the most considered bone in the literature [1–5] and the method used in [6, 7] is now routinely applied in clinical environment.Thus it has been proved to be useful for pre-operative surgical planning but also for patient monitoring. Then, [6, 7] considered a two stage fast reconstruction process (5 minutes for both lower limbs). First, the operator needed to select landmarks

on both images. Based on these landmarks, the femur was parameterized through geometrical primitives and used partial least squares regression associated with moving least squares (MLS) deformation to obtain an initial solution. In a second stage, the operator adjusted the retro projected contours of the initial model comparing to the image contours. This is realized using handles to locally drive the deformation through MLS. This method has been validated regarding the clinical parameters [6, 7], however training is required to expect a trustworthy bone representation. Automation is then appropriate to improve robustness and speed up the process.
Since, several algorithms have been proposed to automate the 3D reconstruction process. A lot of them are based on statistical shape model [3, 8–10], some are based on geometrical primitives parametrization [6, 7], some have a non parametric approach [2, 5]. This last one is contour based and have usually four steps: an initialization, a contour detection, a contour matching and a deformation process like dual kriging [11].

Contour detection is a challenging part in noisy images, in particular when bone structures overlay. A Minimal Path Algorithm (MPA) was introduced by [12] and successfully applied to the femoral head [13]. Also Gaussian Process Regression (GPR) was recently proposed for shape models [14] and can be considered as a generalization of [5]. However, it still might fail in case of multiple contours superimposition. Therefore, we propose here a method combining a modified MPA and GPR.

2. MATERIAL AND METHODS

2.1 Gaussian Process Regression

GPR is a way to predict a posterior shape model composed with n_l 3D anatomical landmarks knowing $m_l \leqslant n_l$ of them.
Let $S_i, i = 1, ..., N$ be N 3D shapes. Each shape model can be represented through a set of corresponding landmarks $(x_k^i, y_k^i, z_k^i) \in \mathbb{R}^3, k = 1, ..., n_l$:

$$S_i = (x_1^i, y_1^i, z_1^i, ..., x_{n_l}^i, y_{n_l}^i, z_{n_l}^i)^T | i = 1, ..., N \tag{1}$$

Therefore, assuming vectors S_i follow a multivariate normal law, $u \sim \mathcal{N}(\mu, K)$, the mean shape model μ and the kernel as the Principal Component Analysis (PCA) covariance matrix can be estimated as (2).

$$\mu = \frac{1}{N}\sum_{i=1}^{N} S_i \text{ and } K = \frac{1}{N}\sum_{i=1}^{N} (S_i - \mu)(S_i - \mu)^T \tag{2}$$

Then, knowing $P = [P_1, P_2, \ldots, P_{m_l}]$, with $p_k \subset \{(x_k^i, y_k^i, z_k^i) \in \mathbb{R}^3 | k = 1, ..., n_l\}$ and assuming $u(p_k) + \varepsilon = \widetilde{u}_k$, with $\varepsilon \sim \mathcal{N}(0, \sigma^2 I_{3m_l})$, GPR evaluates $\forall (x, x') \in GP$ a posterior mean $\overline{\mu}$ and a posterior kernel $\overline{\Sigma}$, with a variance σ^2 related to the accuracy of the input landmarks.

$$\begin{aligned} \overline{\mu}(x) &= \mu(x) + K(x, P)\left(K(P, P) + \sigma^2 I_{3m_l}\right)^{-1}(\widetilde{u} - \mu(P)) \\ \overline{\Sigma}(x, x') &= K(x, x') - K(x, P)\left(K(P, P) + \sigma^2 I_{3m_l}\right)^{-1} K(P, x') \end{aligned} \tag{3}$$

2.2 Subjects and database

GP_1 is built from 120 femurs reconstructed from bi-planar X-rays [16], they are aligned on their barycenter, encoding this way the rigid rotation prior. 50 already segmented femurs were collected from the Virtual Skeleton Database [15]. These femurs are used to build an additional GP_2, they have been registered with the same method than [18] and aligned through the Generalized Procrustes Analysis (GPA).
The second part of our database is dedicated to the validation process and is completely independent from the previous one. 20 femurs were segmented from cadaveric CT-scan (0.75 mm thickness) using MITK-GEM [17] (16 intact and 4 pathologic). 24 (mean age 26.9 year, 12 subjects, 6 males, 6 females) healthy and 16 (mean age 67.5 year, 10 subjects, 6 males, 4 females) pathological (osteoarthritis) femurs were also reconstructed from bi-planar X-rays (0.186 mm resolution) from the method described in [7].

2.3 Initial solution

8 radiologic landmarks (Fig.1) are digitized on each X-rays 1 stereo corresponding (SCP) landmark (1 sphere for the femoral head), 4 Non Stereo Corresponding Points (NSCP) on the frontal view (greater and lesser trochanter and the medio-lateral points of the condyles), 2 on the sagittal view (the two posterior condyles points).

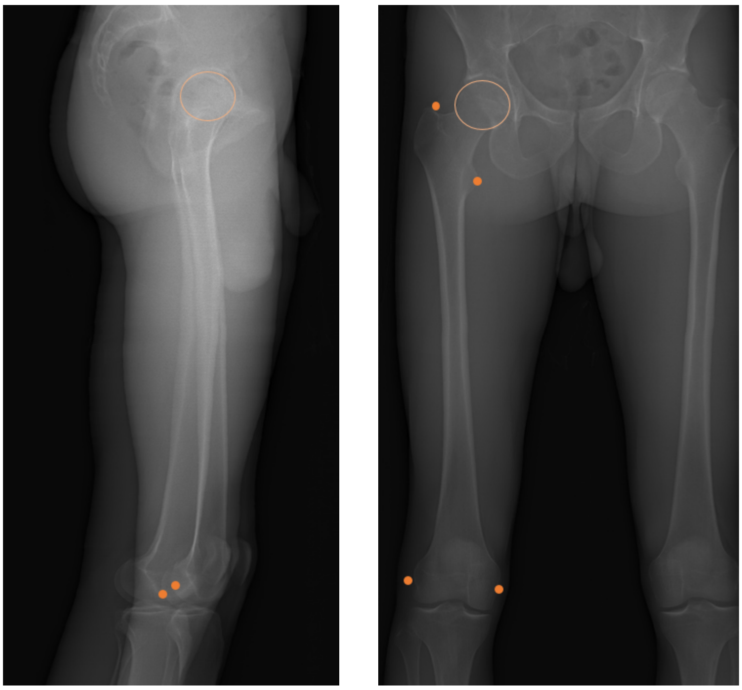

(a) Sagittal view (b) Frontal view

Figure 1. Initial digitalization of the femur from bi-planar X-rays

At this stage, the SCP is used through the GPR using GP_1. One of the landmarks is randomly assigned to the medial posterior points, the other one as the lateral posterior landmark.

Then, 2 successive GPR are applied, using first the posterior points, then the lateral one. Contrary to the previous point, they are NSCP, only the line they belong to are known. Therefore, to get an approximate 3D location of the vertex, the corresponding one on the current femur shape is projected onto this line. The two configurations are tested and the one with the higher probability shape score regarding the GP is kept.

2.4 3D reconstruction algorithm

Once the initial solution is obtained, a modified MPA with three cost maps is applied, followed by a deformation step restricted to some regions R_i depending on the iteration i. While the maximum displacement condition is not reached or $i < 20$, the process iterates again (Fig.2).

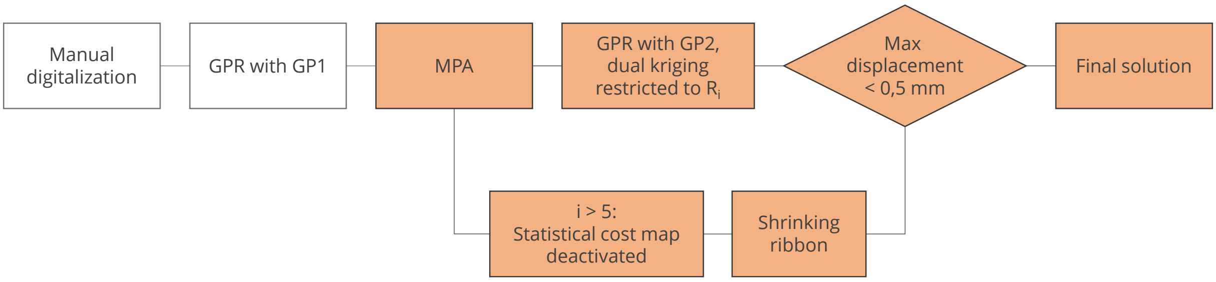

Figure 2. Whole pipeline of the reconstruction process

MPA [12, 13] has been proved to be robust to detect linear features in gray images using an initial solution. Starting from an initial contour, it looks for a similar shape in a user defined range search area. In the contour extraction process of the mesh, two kind of contours are considered, the external ones which basically correspond to the silhouette and the internal ones which are generated from local bumps. Internal contours are computed in a similar way to [10]. The outer contours of the projected mesh are obtained first projecting all triangle faces, then iteratively merging them using Vatti's algorithm [19]. This process ensures a clean silhouette extraction and enables to identify the vertices belonging to this one.

A recursive median filter followed by an adaptive histogram equalizer filter are first applied on the region of interest. Then, as the MPA is graph based, it involves one or several cost maps. The first one, related to the smoothness cost is similar to the one depicted in [13]. The first step aims to straighten a ribbon which medial axis follows the retro-projected contour of the initial solution. In fact, points are regularly samples along the initial contour (Fig.3). Along the ribbon, closest vertices belonging to the contour are merged with the sampled points. Orthogonal lines $n_j \in \mathbb{R}^2$ are then computed going through all the previous points and gray values of the images are resampled along those lines. From the previous interpolated ribbon, the oriented gradient is obtained. Finally the obtained cost map is reverted for the graph minimization solving.

A second type of cost map is introduced to constrain the path to go through digitized landmarks. To do so, we first define the incertitude range related to the operator expected accuracy for each point [20]. Then for all weights of the cost map in this range around the selected landmarks, the new weights values are set as an infinity cost. The neighborhood of the keypoints are also weighted with a Gaussian kernel to smoothly drive the path near the operator selection. The

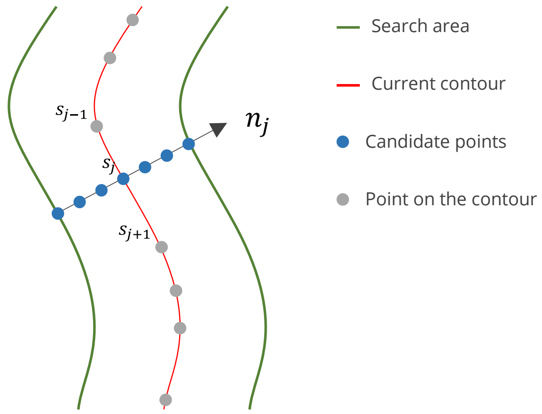

Figure 3. Sampling process of the ribbon

sigma value is the same as the incertitude value.
The last cost map is a statistical one. Actually, to each candidate point on n_j, a constrain line can be associated. And, to each of this constrain line a 3D point can be calculated as the projection of the 3D shape onto this line. Then, considering the posterior GP_1 with a mean $\overline{\mu}$ and a kernel $\overline{\Sigma}$, for two neighbor candidates $(p_1, p_2) \in \mathbb{R}^3$ along n_j, similar to [21], the paired statistical energy is defined as:

$$E_{stat}(p_1, p_2) = \frac{1}{2}\sum_{i=1}^{2}\left(exp\left(-\frac{1}{2}(p_i - \overline{\mu})\overline{\Sigma}^{-1}(p_i - \overline{\mu})^T\right)\right) \tag{4}$$

This energy is particularly efficient to discriminate outliers. For example, on the proximal part, when diaphyses are close from each other, and parallel enough, the statistical cost function ensures the right contour of the right diaphysis is detected. Finally, the directed graph can be solved using dynamic programming as proposed in [13] (Fig.4).

At this stage, the MPA found a contour which follows the gradient edges. Thanks to the sampling process, paired points between the current contour and the one which is detected are automatically set. To compute a plausible new 3D location of each vertex belonging to the contour, the associated one to the current 3D shape is projected on the constraint line coming from the image paired point. The vertices which belong simultaneously to the contour and to the GP_2 are used in the GPR. It is therefore necessary to also rigidly align the new matched vertices coordinates in the GP space. For that reason GPA is realized between the matched vertices and the corresponding mean ones of the GP. To model uncertainty of the new locations of the concerned vertices, anisotropic Gaussian noise is introduced with a variance of 20 mm^2 in the direction of the constrained line, 2 mm^2 otherwise. A second deformation stage is achieved; this time, a dual kriging [11]. This enables to capture finer details and optimize the global position of the bone. Finally, the obtained shape is back projected and the same last steps are applied again.

Because particular matched regions are not reliable at first sight, they are deactivated during the first iterations. For example the lesser trochanter and the anterior distal part near the patella

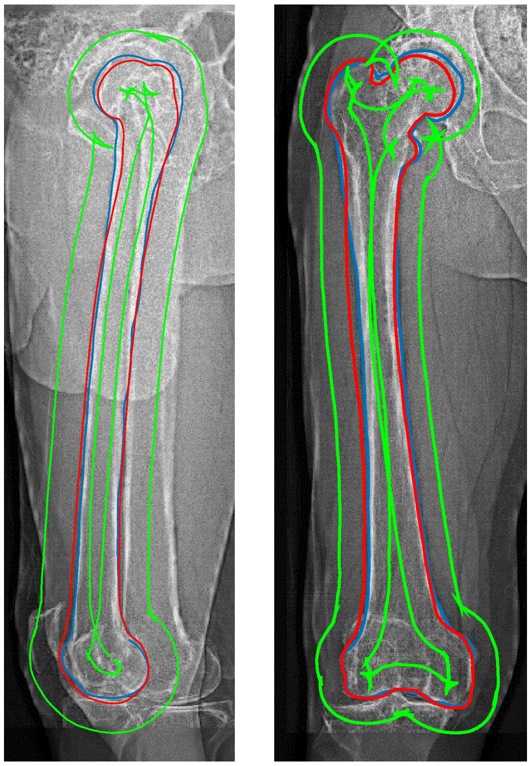

(a) Sagittal view (b) Frontal view

Figure 4. Result of the MPA using the back projected contours of the initial solution - red, contour of the initial solution - green, search area - blue, new detected contour

are activated after 5 iterations. Meanwhile, these regions are driven by the GPR and therefore get closer and closer from the target shape.
Simultaneously to this process, the ribbon is shrinked, discarding outliers in noisy areas. Considering r_{w_0} as the initial ribbon width, s_f the shrinking factor and i the number of iterations,

$$r_w = r_{w_0} {s_f}^i \tag{5}$$

r_{w_0} and s_f are arbitrary defined through a trial-and-error methodology. For instance, r_{w_0} was set to 120 px and s_f to 0.9 for the frontal silhouette.

2.5 Evaluation

The 3D reconstruction has been first evaluated in terms of shape and femoral torsion accuracy. For each cadaveric CT-scan, a 3D mask has been drawn to remove one lower limb, as the two femurs were each time strictly aligned. From these masked 3D volumes digitally reconstructed radiographs (DRR) are created to simulate bi-planar radiographs with the same radiological environment of the EOS (EOS imaging, Paris, France).
The 3D reconstruction of the femur from DRRs was then compared to segmented object considered as the gold standard. As the DRR is generated in the EOS environment, point-to-surface distances can be computed directly. The reconstructed femurs all have the same topological

mesh since they are generated from the GP. Therefore, a distance map is calculated projecting the 2372 vertices onto the target segmentation. At each of these vertices, mean and the RMSE are calculated. The global mean error and the 2 RMSE values are estimated too. Femoral torsion, considered as the major clinical parameter was automatically extracted from both shapes, our 3D reconstruction and the gold standard.
The semi-automated 3D reconstruction has also been evaluated on real bi-planar X-rays. From the database of 40 patients, this method was compared to the fast one [7] in term of femoral torsion. A Bland-Altman plot [22] has also been calculated to compare the two methods.

3. RESULTS

3.1 Comparison to the CT-scan

The point-to-surface distance between the 3D quasi automated reconstruction of the femur (Fig.5), and the 3D reference shows a global mean value of 1.0 mm and 2 RMSE 1.6 mm. We compare favorably to [7]: 0.3 mm less for the global mean and 0.8 mm less for the 2 RMSE. The higher errors appear on the interior part of the greater trochanter. The femoral torsion error are presented through the Bland-Altman plot Fig.6. The bias of the femoral torsion error is reported as 0.1° (2.2° for the fast method) and the 2 standard deviation (SD) as 4.7° (not defined for the fast method).

3.2 Comparison to the previous method

The bias of our computed femoral torsion compared to the fast reconstruction [7] is reported as -1.1° and a 2 SD of 5.5°. As previously, the Bland-Altman plot provides a more detailed overview Fig.7. Note the 2 SD reproducibility error in the fast method was estimated as 3.8°.

4. DISCUSSION

The aim of this study was to fasten the previous reconstruction method using a non ambiguous digitization.

4.1 3D reconstruction method

The fast reconstruction method [7] required two steps: initial solution and contour adjustment. The reconstruction pipeline proposed here only needs 2D digitalization; adjustment is now fully automated reducing operator time. Regarding the initial solution, it is less operator dependent since medio-lateral condyles don't have to be distinguished anymore. Meanwhile, the number of radiological landmarks have been lowered (40 s. to select them).
Moreover, automated segmentation have been achieved combining MPA with different priors, GPR and dual kriging. This overcome the issue of diversity [14] of the database on which usually relies SSM based methods.

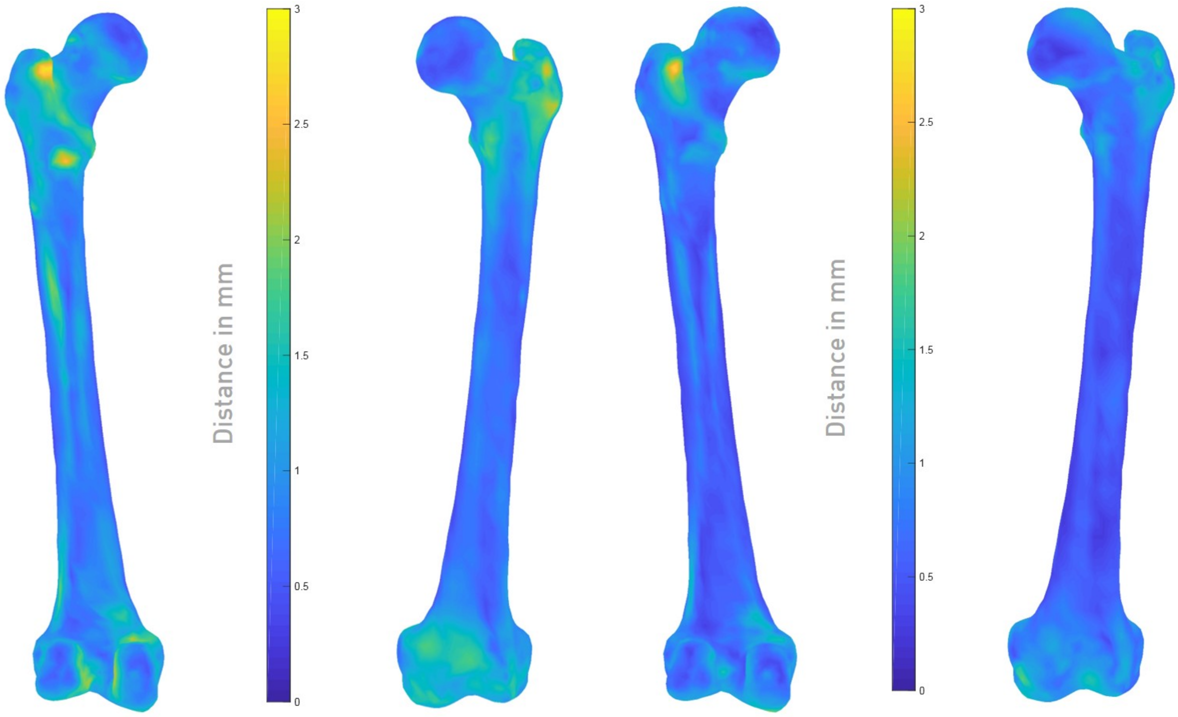

(a) distance map of the mean errors (b) distance map of the RMSE

Figure 5. Points-to-surface metrics comparing the proposed method to the gold standard

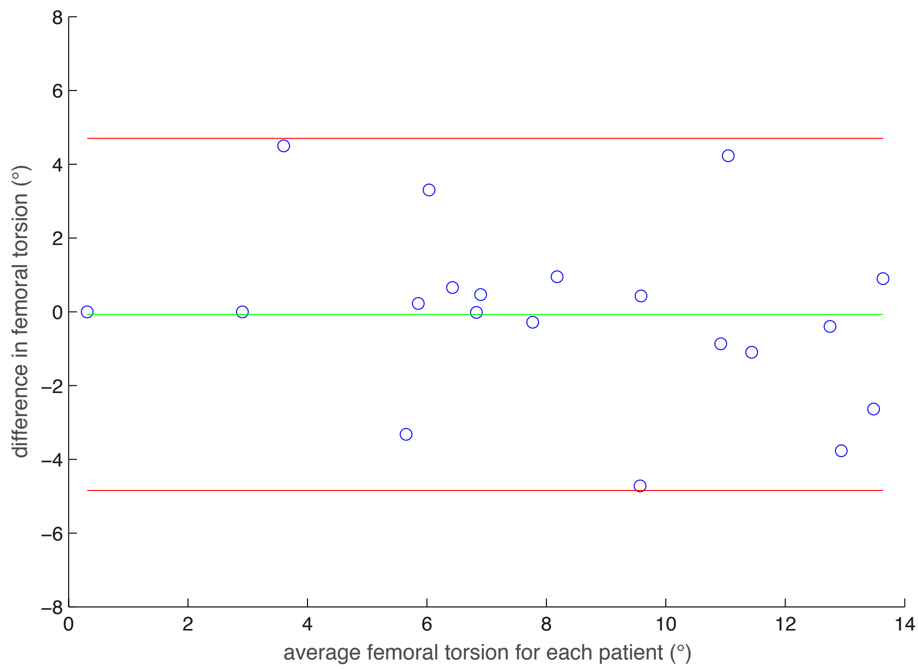

Figure 6. Bland-Altman plot comparing computed femoral torsion from the proposed method to the gold standard - bias in green - 2SD in red

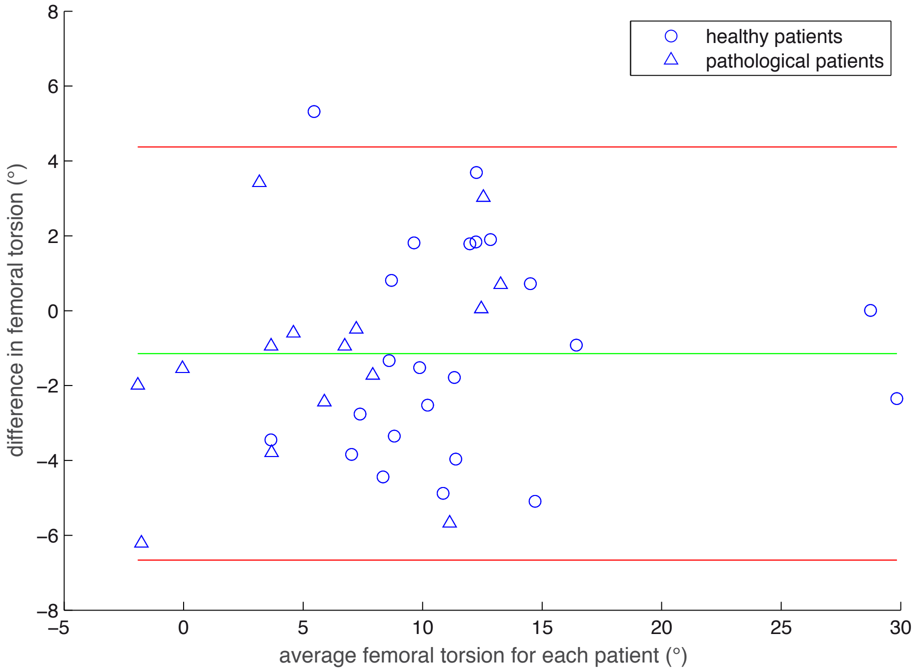

Figure 7. Bland-Altman plot comparing computed femoral torsion from the proposed method to [7] - bias in green - 2SD in red

4.2 Metrics accuracy

Compared to the literature the proposed method is the best compromise between simplicity and robustness. Few studies deal with the entire femur. Among them, in term of points-to-surface distances, they respectively obtained for the mean and 2 RMSE: [9] (1.0 mm, 1.35 mm) [6, 7] (1.0 mm, 2.4 mm), [23] (1.1 mm, 2.8 mm), our method (1.0 mm, 1.6 mm).
Regarding the proposed 3D reconstruction, maximum errors appear on the inner part of great trochanter, but this will not impact clinical parameters. Besides, femoral torsions measured on cadaveric subjects are close from the values obtained with the previous method. We also successfully applied our method in real conditions comparing the femoral torsions to those obtained with [7] and didn't notice any real differences between pathological and healthy patients. However, the errors are a bit higher compared to cadaveric subjects. This might be explained because of the variance cumulation of both methods.

As main limitation of this study, only the femur was considered and not the entire lower-limb. Furthermore, shape accuracy has been only validated on DRR but we expect actually even better results in real clinical environment since bi-planar images have higher contrast and resolution. Finally, adjustment can't be real time controlled yet since the whole process takes 3 min. in a non optimized MATLAB version.

References

[1] P. E. Galibarov, P. J. Prendergast, and A. B. Lennon. A method to reconstruct patient-specific proximal femur surface models from planar pre-operative radiographs. *Medical*

Engineering and Physics, 32(10):1180–1188, 2010.

[2] Vikas Karade and Bhallamudi Ravi. 3d femur model reconstruction from biplane x-ray images: a novel method based on laplacian surface deformation. *International journal of computer assisted radiology and surgery*, 10(4):473–85, 4 2015.

[3] N. Baka, B. L. Kaptein, M. de Bruijne, T. van Walsum, J. E. Giphart, W. J. Niessen, and B. P F Lelieveldt. 2d-3d shape reconstruction of the distal femur from stereo x-ray imaging using statistical shape models. *Medical Image Analysis*, 15(6):840–850, 2011.

[4] Sonia Akkoul, Adel Hafiane, Olivier Rozenbaum, Eric Lespessailles, and Rachid Jennane. 3d reconstruction of the proximal femur shape from few pairs of x-ray radiographs. *Signal Processing: Image Communication*, 2017.

[5] S Laporte, W Skalli, J a de Guise, F Lavaste, and D Mitton. A biplanar reconstruction method based on 2d and 3d contours: application to the distal femur. *Computer methods in biomechanics and biomedical engineering*, 6(1):1–6, 2003.

[6] Y. Chaibi, T. Cresson, B. Aubert, J. Hausselle, P. Neyret, O. Hauger, J. A. de Guise, and W. Skalli. Fast 3d reconstruction of the lower limb using a parametric model and statistical inferences and clinical measurements calculation from biplanar x-rays. *Computer Methods in Biomechanics and Biomedical Engineering*, 15(5):457–466, 2012.

[7] S. Quijano, A. Serrurier, B. Aubert, S. Laporte, P. Thoreux, and W. Skalli. Three-dimensional reconstruction of the lower limb from biplanar calibrated radiographs. *Medical Engineering and Physics*, 35(12):1703–1712, 2013.

[8] Ofri Sadowsky, Gouthami Chintalapani, Russell H. Taylor, M. J. van der Bom, J. P. W. Pluim, R. Homan, J. Timmer, and L. W. Bartels. Deformable 2d-3d registration of the pelvis with a limited field of view, using shape statistics. *Lecture Notes in Computer Science (including subseries Lecture Notes in Artificial Intelligence and Lecture Notes in Bioinformatics)*, 6512(Pt 2):65120B–65120B–9, 2007.

[9] Ondrej Klima, Petr Kleparnik, Michal Spanel, and Pavel Zemcik. Intensity-based femoral atlas 2d/3d registration using levenberg-marquardt optimisation. *Proceedings of the SPIE, Volume 9788, id. 97880F 12 pp. (2016).*, 9788:97880F, 3 2016.

[10] Xiao Dong, Miguel Ángel A. González Ballester, and Guoyan Zheng. Automatic extraction of femur contours from calibrated x-ray images using statistical information. *Journal of Multimedia*, 2(5):46–54, 2007.

[11] F. Trochu. A contouring program based on dual kriging interpolation. *Engineering with Computers*, 9:160–177, 1993.

[12] L Vincent. Minimal path algorithms for the robust detection of linear features in gray images. *Ismm*, 12:331–338, 1998.

[13] Fatma Ouertani, Carlos Vazquez, Thierry Cresson, and Jacques De Guise. Simultaneous extraction of two adjacent bony structures in x-ray images: Application to hip joint segmentation. *Proceedings - International Conference on Image Processing, ICIP*, 2015-Decem(January):4555–4559, 2015.

[14] Marcel Lüthi, Christoph Jud, Thomas Gerig, Thomas Vetter, Marcel Luthi, Thomas Gerig, Christoph Jud, and Thomas Vetter. Gaussian process morphable models. *IEEE Transactions on Pattern Analysis and Machine Intelligence*, 8828(April):1–38, 2016.

[15] Michael Kistler, Serena Bonaretti, Marcel Pfahrer, Roman Niklaus, and Philippe Büchler. The virtual skeleton database: An open access repository for biomedical research and collaboration. *Journal of Medical Internet Research*, 15(11), 2013.

[16] A. Nerot, W. Skalli, and X. Wang. Estimation of spinal joint centers from external back profile and anatomical landmarks. *Journal of Biomechanics*, 11 2017.

[17] Yves Pauchard, Thomas Fitze, Diego Browarnik, Amiraslan Eskandari, Irene Pauchard, William Enns-Bray, Halldór Pálsson, Sigurdur Sigurdsson, Stephen J. Ferguson, Tamara B. Harris, Vilmundur Gudnason, and Benedikt Helgason. Interactive graph-cut segmentation for fast creation of finite element models from clinical ct data for hip fracture prediction. *Computer Methods in Biomechanics and Biomedical Engineering*, 19(16):1693–1703, 2016.

[18] Stefan Schlager and Alexandra Rüdell. Sexual dimorphism and population affinity in the human zygomatic structure-comparing surface to outline data. *Anatomical Record*, 300(1):226–237, 2017.

[19] Bala R. Vatti. A generic solution to polygon clipping. *Communications of the ACM*, 35(7):56–63, 1992.

[20] B. Schlatterer, I. Suedhoff, X. Bonnet, Y. Catonne, M. Maestro, and W. Skalli. Skeletal landmarks for tkr implantations: Evaluation of their accuracy using eos imaging acquisition system. *Orthopaedics and Traumatology: Surgery and Research*, 95(1):2–11, 2009.

[21] Junbin Huang, James F. Griffith, Defeng Wang, and Lin Shi. Graph-cut-based segmentation of proximal femur from computed tomography images with shape prior. *Journal of Medical and Biological Engineering*, 35(5):594–607, 2015.

[22] D. G. Altman and J. M. Bland. Measurement in medicine: The analysis of method comparison studies. *The Statistician*, 32(3):307, 1983.

[23] Guoyan Zheng. Statistical deformable model-based reconstruction of a patient-specific surface model from single standard x-ray radiograph. *Lecture Notes in Computer Science (including subseries Lecture Notes in Artificial Intelligence and Lecture Notes in Bioinformatics)*, 5702 LNCS:672–679, 2009.